CSMA 2017
13ème Colloque National en Calcul des Structures
15-19 Mai 2017, Presqu'île de Giens (Var)

On the uniqueness of the elastoplastic properties identified from the indentation test on materials following the Vocé hardening law

L. Meng[1], P. Breitkopf[1], B. Raghavan[2], O. Bartier[3], X. Hernot[3], G. Mauvoisin[3]

[1] *Laboratoire Roberval, UMR 7337 UTC-CNRS, Université de Technologie de Compiègne, Compiègne, France, liang.meng@utc.fr*
[2] *Laboratoire de Génie Civil et Génie Mécanique EA 3913, INSA de Rennes, 20 Avenue des Buttes de Coesmes, 35708 Rennes, France*
[3] *Laboratoire de Génie Civil et Génie Mécanique EA 3913,Université de Rennes 1, 9 rue Jean Macé, 35000 Rennes, France*

Résumé — In this work, we conduct an in-depth investigation of the well-known problem of non-unique solutions to the inverse identification problem for indentation-based characterization, with particular attention to materials following the Vocé law. Knowing the non-unicity of the solution obtained with conical indenters, we preferentially use spherical indenters instead so as to involve an additional length scale. To focus on the nature of the design problem (i.e. well posed or not) independently of experimental errors, the identification is performed using "noise-free" simulated imprint shapes.
Mots clés — Inverse problem, indentation, manifold-learning, Vocé law.

1 Introduction

One of the key advantages of indentation-based characterization is its ability to retrieve a considerable number of mechanical properties for a variety of materials while still being "non-destructive" in nature. That being said, the quality of the solutions obtained has consistently been called into question, given that the final inverse identification problem appears to be, at least in most cases, ill-posed, rendering the obtained solutions non-unique.

The literature available on indentation-based mechanical characterization seems to indicate that the non-unicity of the solution to the final inverse identification problem is now a focal point of research interest. After years of study, it is now widely recognized that the non-uniqueness issue is particularly severe when we use self-similar indenters (conical) for the calibration of the well-known two-parameter Hollomon's (power) law. We note further that this conclusion is relevant only to identification using the indentation load-displacement (P-h) curve, i.e. without taking into account the residual imprint post-indentation.

Chen *et al.* [1] attributed this difficulty, at least in part, to the absence of an explicit relationship between a material's elastoplastic parameters and its indentation response. They proposed a series of explicit formulations to determine the so-called "mystical material" sets with distinct elastoplastic properties but near-indistinguishable P-h curves. By explicitly enforcing constraints on the curvature of the loading curve and the ratio of loading/unloading work and using a *conical* indenter, near-indistinguishable "mystical material" pairs were obtained. Then, to tackle this problem, they recommended using dual sharp and spherical indentation, both of which are capable of yielding a *unique* combination of material properties. The efficiency of these two protocols has been validated by several other authors in the literature.

It is all too clear that the overwhelming majority of the indentation-based identification methods reported in the literature so far have been based on exploiting solely the P-h curve, *ergo* the non-uniqueness issue has, thus far, been only understood in the context of the P-h curve rather than that of the residual imprint profile. On the other hand, recent research indicates that many important engineering materials deviate significantly from simple power law hardening.

With this in mind, we focus here on materials following Vocé hardening with a saturation stress at high strains. We limit ourselves to spherical indentation so as to consider an additional length scale, giving special attention to the existence of *non unique* solutions to the inverse problem, and examine the source of this issue. The identification is performed using the shape manifold concept and a variety of non-linear manifold learning algorithms developed by our research group [2, 3].

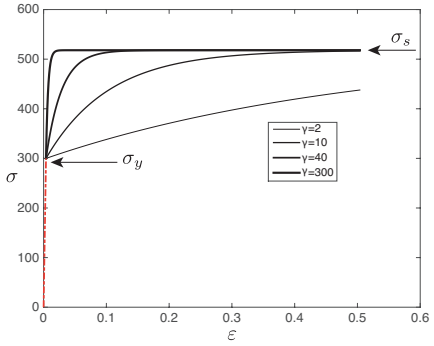

FIGURE 1 – Vocé law defined on three parameters

2 Overall concept and formulation

2.1 Material model

As mentioned in the preamble, instead of the Hollomon's hardening law adopted in [2] and most, if not all the papers in the literature surveyed, we focus here on the Vocé law which involves an additional elastoplastic parameter. From [5], the uniaxial constitutive behavior is represented by the following equation

$$\begin{cases} \sigma = E\varepsilon \\ \sigma = \frac{\sigma_y}{1-m_1}(1-m_1 e^{-m_2\varepsilon_p}) \end{cases}, \tag{1}$$

where E is the Young's modulus (considered as known a priori in current work), ε refers to the total strain, ε_p the plastic stain, σ_y the elastic limit and m_1, m_2 are two dimensionless material parameters which define the hardening behavior. Some authors adopt a terminology involving a "saturation stress" σ_s so as to give a physical meaning to the parameters. The plastic portion of this law may be written as :

$$\sigma = \sigma_y + Q(1-e^{-\gamma\varepsilon_p}). \tag{2}$$

Here, $Q = \sigma_s - \sigma_y$ is the difference between σ_s and initial elastic limit. Essentially, Q is a function of σ_y and m_1, reading $Q = \frac{m_1}{1-m_1}\sigma_y$. Like m_2 in (1), the parameter γ controls how "rapidly" the stress approaches the saturation level. As can be seen in Fig.1, the parameter γ may vary in a rather large range, from 2 to several hundred. This range is wide enough to accommodate the vast majority of engineering materials showing hardening behavior. For example, the constitutive relation illustrates a bilinear elasto-plastic behavior as γ reduces to 2, while an elastic-perfectly plastic behavior is approximated by $\gamma = 300$. In current work, for the sake of clarity, we employ (2) and assign large ranges of variation to σ_y and Q so as to allow for various different materials.

2.2 Finite element model

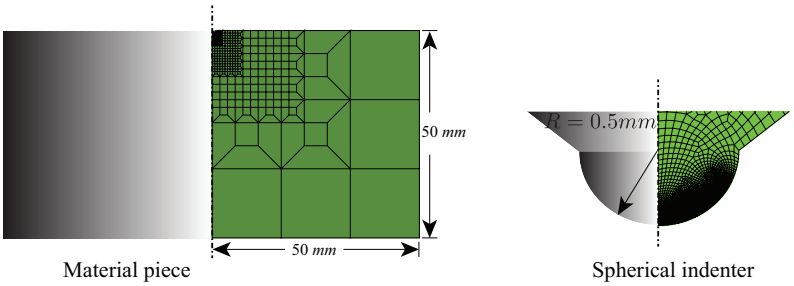

FIGURE 2 – Finite element model of specimen and a spherical indenter tip.

The FE meshes for both indenter and the specimen are shown in Fig.2. We use a denser mesh in the region of interest around the contact zone. Also, for better agreement with the semi-infinite domain assumption, we choose a rather large specimen size $50mm \times 50mm$. Axisymmetric boundary conditions

are applied in view of the geometric symmetry of both the specimen and the indenter. The indentation procedure is modeled assuming finite strains, using ABAQUS/Standard with 4394 four-noded axisymmetric elements CAX4R for the specimen and 6070 elements for the spherical indenter. The contact interface between the two pieces is characterized by a Coulomb friction coefficient c which is set to 0.2. For the indenter, we use the elastic properties of Tungsten Carbide, i.e. Young's modulus $E_i = 600GPa$ and Poisson's ratio $\nu_i = 0.23$. The three Vocé hardening parameters describing the plastic behavior (i.e. other than the elastic properties E) need to be identified.

2.3 Identification in Reduced-order space

We basically apply the method of Proper Orthogonal Decomposition (POD) to the collection of imprint shapes obtained by a series of indentation tests, corresponding to a set of M numerical experiments obtained by an appropriate Design of Experiments for the 3 varying material parameters (σ_y,Q and γ). The different imprint shapes are extracted from the FE simulation results and each is considered as a snapshot $\mathbf{s}_i, i = 1,2\cdots M$. The snapshot matrix $\mathbf{S}$ is then generated from the centered snapshots

$$\mathbf{S} = [\mathbf{s}_1 - \bar{\mathbf{s}}, \mathbf{s}_2 - \bar{\mathbf{s}}, \cdots \mathbf{s}_M - \bar{\mathbf{s}}], \tag{3}$$

where $\bar{\mathbf{s}}$ is the mean snapshot $\bar{\mathbf{s}} = \frac{1}{M}\sum_{i=1}^{M} \mathbf{s}_i$. We then use POD to obtain the reduced-order vector space in which the imprint shape evolves. Singular value decomposition of $\mathbf{S}$ yields

$$\mathbf{S} = \mathbf{\Phi D V^T}, \tag{4}$$

where $\mathbf{D}$ contains the singular values d_i ; each column of $\mathbf{\Phi}$ being an eigenvector of the covariance matrix $\mathbf{C} = \mathbf{SS^T}$, with $\lambda_i = d_i^2$ as the corresponding eigenvalues. These eigenvectors ϕ_i are generally called the POD modes. Each snapshot $\mathbf{s}_i$ may then be accurately reconstructed by using the projection basis $\mathbf{\Phi} = [\phi_1, \phi_2 \cdots \phi_M]$

$$\mathbf{s}_i = \bar{\mathbf{s}} + \mathbf{\Phi}\boldsymbol{\alpha}^i = \bar{\mathbf{s}} + \sum_{j=1}^{M} \alpha_j^i \phi_j, \tag{5}$$

where α_j^i is the projection coefficient (or the coordinates in reduced space) for the i^{th} snapshot on the j^{th} mode, given

$$\alpha_j^i = \phi_j^{\mathbf{T}}(\mathbf{s}_i - \bar{\mathbf{s}}), j = 1,2\cdots M. \tag{6}$$

By combining (3)-(6), a one-to-one correspondence is thus built up between higher-dimensional indentation responses and lower-dimensional coordinates of the new space. We note here that the indentation response $\mathbf{s}_i$ is not limited to the imprint mappings, it could also be the corresponding indentation curves, or even a combination of the two.

In this constructed low-dimensional space, a predictor-corrector manifold walking algorithm (previously proposed in [3]) is used to iteratively locate the local manifold in the vicinity of the projection of the target imprint shape (the target is usually an experimental shape, but we have used a simulated imprint for the reasons described in the abstract and introduction).

3 Numerical test-case

3.1 Non-unicity in the identification of Vocé hardening parameters

In this section, we will attempt to identify the three-parameter Vocé law within the reduced-order space constructed by following the procedures described in Sect.2.3. Since the residual imprint shape outperformed the loading-unloading curve for identifying Hollomon's power law parameters, we will use the imprint shape correlation approach for the identification. The corresponding P-h curves will be compared only at convergence purely for the purpose of verification. Again, we use a numerical imprint as the target shape, and the "pseudo-experimental" response is simply an FE simulation using the model presented in Sect.2.2, with a maximal penetration depth $h_{max} = 0.1mm$, and using : $\sigma_y^{ref} = 300$MPa, $Q^{ref} = 200$MPa ($\sigma_s = 500$MPa) and $\gamma^{ref} = 14$. Using the local manifold learning "Floating search" algorithm [2, 3], we intend to identify the three "missing" constitutive parameters.

An arbitrarily chosen combination of constitutive parameters A : $(\sigma_y, Q, \gamma) = (430, 350, 100)$ is set as the initial point. In Fig.3, we present the convergence histories for the three Vocé parameters, normalized by their corresponding reference/nominal values, σ_y^{ref}, Q^{ref} and γ^{ref}. We observe that by beginning the search from A, we retrieve the three parameters with reasonable accuracy at the end of 16 iterations, with a maximum error of 2.14% being observed for the third parameter γ (by comparing with their reference values) in Tab.1.

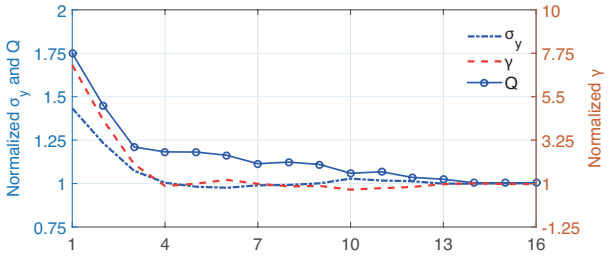

FIGURE 3 – Convergence summary for the three Vocé parameters normalized by their corresponding referential values (initial point A : $(\sigma_y, Q, \gamma) = (430, 350, 100)$).

Next, to rule out any possible influence of the choice of the initial point in inverse optimization, we assign *another* arbitrarily chosen combination of material parameters B : $(\sigma_y, Q, \gamma) = (200, 600, 140)$ as the new initial point for the algorithm. The new convergence histories for the three parameters are shown in Fig.4, and the final identified values obtained are compared with that obtained by starting from A, in Tab.1. As seen in Fig.4, despite all three parameters clearly stabilizing around a particular set of values, only ONE of them (Q) is probed correctly when compared to the reference value. Large deviations from the reference values are seen for the two other parameters, γ in particular with an error of up to 200% !

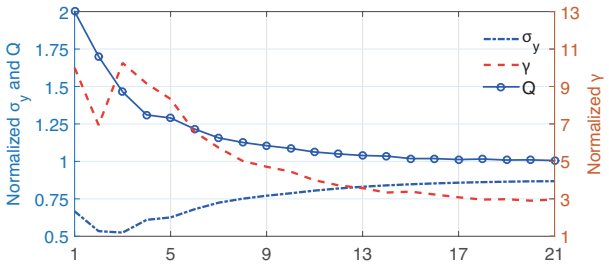

FIGURE 4 – Convergence summary for the three Vocé parameters normalized by their corresponding referential values (initial point B : $(\sigma_y, Q, \gamma) = (200, 600, 140)$).

TABLE 1 – Recovered Vocé parameters through different initial iteration points. The results are for a solid with E and ν fixed at 70GPa and 0.3, respectively.

Case	σ_y (MPa)	$\%err$ σ_y	Q (MPa)	$\%err$ Q	γ	$\%err$ γ
A	300.50	0.17%	200.88	0.44%	13.70	2.14%
B	260.29	13.24%	201.15	0.57%	41.50	196.43%

We observe that it appears to be difficult to accurately identify subtle differences in the post-yield properties using only the indentation imprint. In other words, the two identified parameter sets belong to a so-called "mystical pair" of materials, both of which ostensibly minimizing the discrepancy with the "experimental" imprint.

As mentioned previously, the corresponding indentation P-h curves will now be compared to check whether the two "mystical sibling" materials can still be distinguished by using other indentation responses. Unfortunately, we note in Fig.5, that the two indentation curves are nearly overlapping despite the constitutive behaviors of the two materials being clearly distinct from each other (inset on top-left corner). Even though, as reported in [4], the combination of P-h curve and imprint can sometimes render the inverse problem slightly better-posed, this combination seems to be meaningless in the current

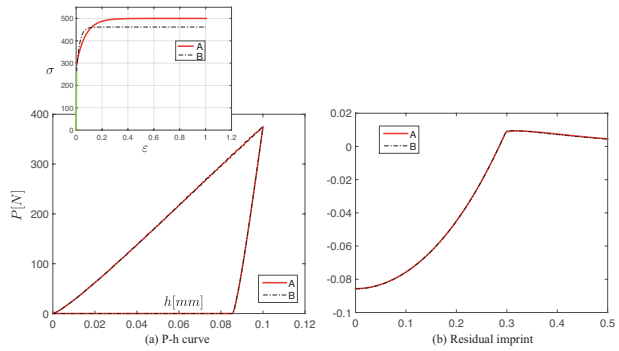

FIGURE 5 – Comparison of indentation responses of *mystical* materials.

case wherein both the indentation curves and the residual imprints are indistinguishable using a spherical indenter.

The question then is, where does this problem of non-unicity arise ? Is this failure in characterization due to the inefficiency of the optimization algorithm used in the inverse analysis, or simply because the collected/measured information from the indentation response does not adequately interpret *all* material plasticity ? This question will be answered in the follow subsections by comparing a series of manifolds built on different synthetic i.e. simulated indentation responses.

3.2 Verification of the efficiency of the manifold identification procedure

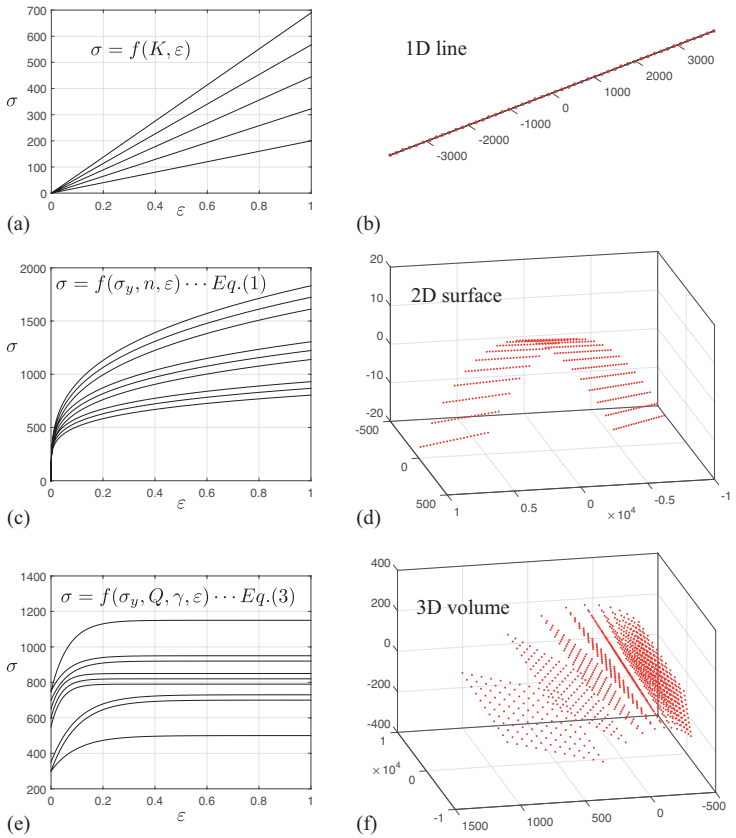

FIGURE 6 – Illustrative stress-strain curves and the corresponding manifolds built without FE simulations : (a)-(b) for Hooke's law, (c)-(d) for Hollomon's law, and (e)-(f) Vocé law.

To verify the manifold identification protocol, we first *directly* use the constitutive behavior itself as defined by the corresponding material parameters to construct the low-dimensional manifold, i.e. without indentation. This simply means that, in lieu of the indentation response (imprint shape), we use the $\sigma - \varepsilon$ curve itself as a "special shape" and used for the POD snapshots. For comparison, we study

the one-parameter (Young's modulus E) Hooke's law, the two-parameter (σ_y and n) Hollomon's and the three-parameter (σ_y, Q and γ in (2)) Vocé law. Sufficiently large parameter intervals are chosen for the Design of Experiments : $E \in [200\text{Gpa}, 800\text{Gpa}]$ for Hooke's law, $\sigma_y \in [200, 240]$ and $n \in [0.2, 0.3]$ for Hollomon's power law, and $\sigma_y \in [300, 800]$, $Q \in [200, 400]$ and $\gamma \in [10, 60]$ for Vocé hardening law.

On the left of Fig.6, we show a series of representative stress-strain curves for the 3 different material constitutive laws. As indicated, all the curves in Fig.6.(a) are generated varying the only parameter E, and the constructed manifold is revealed to be a straight line, as in Fig.6.(b). Using the hypothesis of the manifold [2], the stress-strain behavior of any other elastic material lay then be projected as a single point lying *on* this line, and the identification of the parameter E will be done simply by interpolating the points.

Similarly, all the curves in Fig.6 (c) are governed by the two parameters of the Hollomon's power law, σ_y and n, and as expected, the constructed manifold shows a feature of a 2D surface. As observed, the projections of different material properties are arranged in a regular fashion on the manifold, allowing us to once again use interpolation to probe the properties of a given target material.

Finally, for the Vocé law defined by σ_y, Q and γ, the stress is constricted by a clear saturation stress at high strain level, see Fig.6 (e), and we clearly observe that the corresponding manifold in the reduced space is a 3D cloud of points, Fig.6 (f), indicating that all three parameters are independent (as they should be) and we can identify them correctly and *uniquely* from the stress-strain curve.

For the sake of completeness, we carry out eight different identification procedures for the Vocé parameters by directly using the constitutive law "special shape" with different starting points. The $\sigma - \varepsilon$ curve obtained from the set $(\sigma_y, Q, \gamma) = (300, 200, 25)$ is used as the "*target shape*", and the parameter set to be identified is located (by design) at the centroid of the cube enclosed by the eight initial points as vertices, as illustrated in Fig.7. Tab.2 lists the final estimates for the three parameters and the number of iteration steps for each corresponding case. We note that, in all eight cases, we always converge to a *unique* combination of parameters. A maximal difference of 0.16% and 0.1% are observed for γ and Q respectively, with respect to their target values.

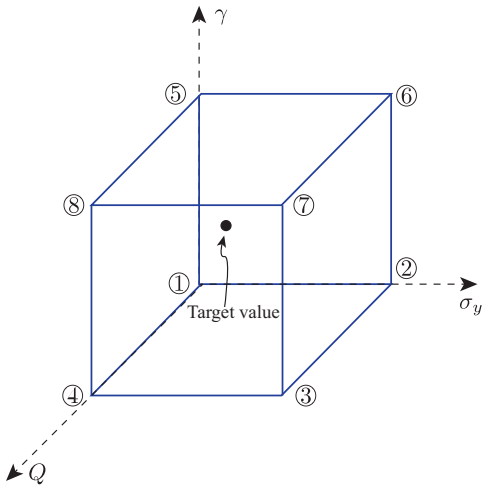

	σ_y	Q	γ
①	100	100	10
②	500	100	10
③	500	300	10
④	100	300	10
⑤	100	100	40
⑥	500	100	40
⑦	500	300	40
⑧	100	300	40
●	300	200	25

FIGURE 7 – Eight different initial iteration points defined in parameter space.

We conclude therefore that the number of identifiable parameters may be estimated by the dimensionality of corresponding manifold, confirming the manifold hypothesis. This inference may be readily verified from the manifolds presented in Fig.6 and the corresponding identification results. While we are aware that no iteration is required to probe material parameters from the uniaxial stress-strain constitutive law and the identification can be readily accomplished by curve fitting provided that the target $\sigma - \varepsilon$ curve has already been obtained from a tensile test. That said, the identification procedures presented above, though redundant and bordering on overkill for this simple problem, still help us to rule out the possibility of any inefficiency or other issues surrounding either the manifold hypothesis or the manifold learning algorithm.

TABLE 2 – Vocé parameters identified through stress-strain curve with different iteration staring points.

Initial points	σ_y	Q	γ	Iter No.
①	299.96	200.08%	25.02	34
②	300.08	199.86%	24.96	34
③	299.92	200.12%	25.04	25
④	299.93	200.10%	25.04	21
⑤	299.93	200.19%	25.03	23
⑥	299.97	200.03%	25.02	28
⑦	299.96	200.11%	25.02	23
⑧	300.02	199.95%	24.99	33
References	300	200	25	–
Max error	0.03%	0.10%	0.16%	–

3.3 The shortcomings of indentation as a method of characterization

In the current section, an analogous procedure to the one explained in Sect.3.2 is followed with consideration of indentation responses rather than $\sigma - \varepsilon$ curve. Following our previous research, we preferentially use the residual imprint profiles upon withdrawal of the spherical indenter in order to obtain more information about the material's plastic behavior after indentation. For the Hooke's law, we need only the indentation curve since no plastic deformation is present after unloading, i.e. no imprint, regardless of the choice of maximum penetration depth. In any case, unlike standard indentation curves, the loading and unloading portions overlap for perfectly elastic materials.

On the left of Fig.8, we show a collection of representative indentation P-h curves and/or residual imprints corresponding to the three chosen material laws. The constructed manifolds are shown on the right. It is observed in Fig.8 (b) that, once again, the manifold for Hooke's law is a straight line. While the distribution of the various indentation curves is slightly different from that shown in Fig.6 (b), it is

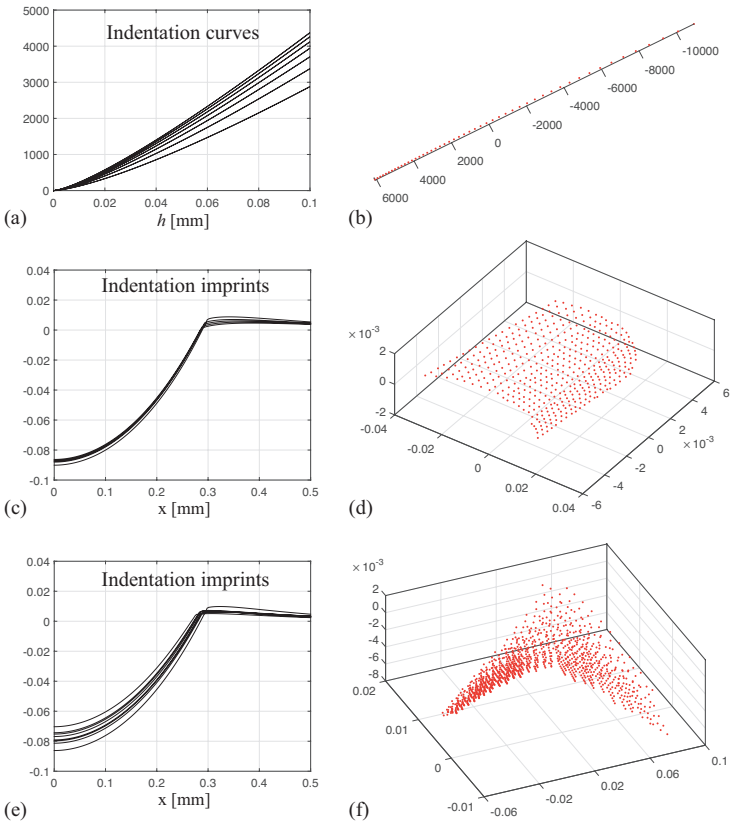

FIGURE 8 – Indentation responses and different manifolds built based on : (a)-(b) Hooke's law, (c)-(d) Hollomon's law, and (e)-(f) Vocé law.

however quite understandable that this is due to the fact that slight variations in the Young's modulus$E$ (i.e., ΔE in DoE sampling) do not always lead to the same variation in the indentation curve. By examining the elastic properties, we find that the materials (represented by their modulus) located in the dense zone of the manifold correspond to extreme hard materials (with higher E). In any case, the one-to-one correspondence between parameter values for E and the indentation curve is still valid for this first case.

Next, we consider materials hardening according to Hollomon's power law, the manifold in Fig.8 (d) suggests that the non-unicity issue does not present itself in this case either. The two parameters can be easily identified from a measured indentation imprint. In this illustrative case, we adopt a spherical indenter, but even with a single conical indenter, similar results are obtained. This is explained by the fact that material plasticity is, in most cases, better interpreted from the residual imprint than from the P-h curve, during indentation-based characterization. This is discussed at length in our previous work [4] along with a discussion of the effect of the shape of the indenter.

For materials hardening according to the three-parameter Vocé law on the other hand, when we map the imprint mappings (that should be governed by three parameters) we obtain a quasi-2D manifold, Fig.8 (f) ! This *may* signify a possible *inter-dependence* of the material parameters in the indentation responses, or in other words, the influences of the variations of the different parameters on indentation imprint may actually be nullified by each other. As a consequence, the combination of material parameters identified assuming the Vocé law is likely unreliable. This insight gleaned from the manifold of indentation imprints turns to be reconciled with the non-unique identification of Vocé parameters detailed in Sect.3.1. On the other hand, we build the manifold using indentation P-h curves as well, however, a similar manifold as that obtained using the imprints is obtained.

For these reasons, we must question whether simply relying only on the indentation test is sufficient to characterizing Vocé hardening materials, or if supplementary material data from other experimental techniques (other than indentation) would be required.

4 Conclusions and perspectives

The objective of this work was to shed some light on the non-unicity problem faced during characterization by indentation, with special attention paid to the identification of Vocé law materials.

We demonstrate, by solving the inverse problem using the shape manifold and associated learning algorithms, that the so-called "mystical material" pairs do exist. By explicitly comparing the 3D manifolds considering directly the constitutive law itself as a "shape" with those obtained from the indentation responses for three different constitutive laws, we feel that the failure of identification is not due to the inefficiency of the identification protocol, but rather a direct consequence caused by the *"averaged"* indentation response.

As future work, we recommend that the characterization of Vocé parameters by the indentation test, hitherto given almost no attention in the literature, should be studied in more detail.

Références

[1] X, Chen, N, Ogasawara, M, Zhao, et al. *On the uniqueness of measuring elastoplastic properties from indentation : the indistinguishable mystical materials*. Journal of the Mechanics and Physics of Solids, 55(8) : 1618-1660, 2007.

[2] L. Meng, P. Breitkopf, B. Raghavan, et al. *Identification of material properties using indentation test and shape manifold learning approach*, Computer Methods in Applied Mechanics and Engineering, 297 : 239-257, 2015.

[3] L. Meng, P. Breitkopf, B. Raghavan, et al. *Nonlinear Shape-Manifold Learning Approach : Concepts, Tools and Applications*. Archives of Computational Methods in Engineering, 1-21, 2016.

[4] L. Meng, P. Breitkopf et al. *An insight into the identifiability of material properties by instrumented indentation test using manifold approach based on P-h curve and imprint shape*, International Journal of Solids and Structures, 106 : 13-26, 2017.

[5] C. Zhang, B. Wang. *Identification of the hardening behavior of solids described by three-parameter Vocé law using spherical indentation*. Journal of Materials Research, 27(20) : 2624-2629, 2012.